Non-contact detection of myocardium's mechanical activity by ultrawideband RF-radar and interpretation applying electrocardiography

F. Thiel,[a] D. Kreiseler, and F. Seifert
Physikalisch-Technische Bundesanstalt (PTB), Abbestr. 2-12, 10587 Berlin, Germany

(Received 22 June 2009; accepted 7 September 2009; published online 10 November 2009)

Electromagnetic waves can propagate through the body and are reflected at interfaces between materials with different dielectric properties. Therefore the reason for using ultrawideband (UWB) radar for probing the human body in the frequency range from 100 MHz up to 10 GHz is obvious and suggests an ability to monitor the motion of organs within the human body as well as obtaining images of internal structures. The specific advantages of UWB sensors are high temporal and spatial resolutions, penetration into object, low integral power, and compatibility with established narrowband systems. The sensitivity to ultralow power signals makes them suitable for human medical applications including mobile and continuous noncontact supervision of vital functions. Since no ionizing radiation is used, and due to the ultralow specific absorption rate applied, UWB techniques permit noninvasive sensing with no potential risks. This research aims at the synergetic use of UWB sounding combined with magnetic resonance imaging (MRI) to gain complementary information for improved functional diagnosis and imaging, especially to accelerate and enhance cardiac MRI by applying UWB radar as a noncontact navigator of myocardial contraction. To this end a sound understanding of how myocardial's mechanic is rendered by reflected and postprocessed UWB radar signals must be achieved. Therefore, we have executed the simultaneous acquisition and evaluation of radar signals with signals from a high-resolution electrocardiogram. The noncontact UWB illumination was done from several radiographic standard positions to monitor selected superficial myocardial areas during the cyclic physiological myocardial deformation in three different respiratory states. From our findings we could conclude that UWB radar can serve as a navigator technique for high and ultrahigh field magnetic resonance imaging and can be beneficial preserving the high resolution capability of this imaging modality. Furthermore it can potentially be used to support standard electrocardiography (ECG) analysis by complementary information where sole ECG analysis fails, e.g., electromechanical dissociation.
 [doi:10.1063/1.3238506]

I. INTRODUCTION

Noncontact detection and monitoring of human cardiopulmonary activity through bedding and clothing would be a valuable tool in intensive care monitoring and home health care applications. Patients with conditions that can be perturbed or worsened by contact sensors include neonates, infants at risk of sudden infant death syndrome, and burn victims; a noncontact heart and respiration rate monitor could provide vital signs monitoring without affixed electrodes for these patients. Most alternatives to standard heart and respiration monitors need leads and contacts and often require accurate control or placement. This may be impossible or undesirable in many situations.[1]

Our research aims at the synergetic technological development of noncontact ultrawideband (UWB) sounding combined with magnetic resonance imaging (MRI), to explore its efficacy in such innovative fields of application as the imaging of coronary arteries, heart beat monitoring, and accurate modeling of electromagnetic wave propagation through heterogeneous, biological tissue. MRI is not *per se* capable of creating focused images of moving organs like the myocardium or the thorax during respiration. Rather, additional techniques are required. Usually, MRI uses electrocardiography (ECG) information to acquire an image over multiple cardiac cycles by collecting segments of *k*-space at the same delay within the cycle. This requires breath hold as it is assumed that cardiac positions are reproducible over several ECG cycles. Unfortunately, in clinical situations, many subjects are unable to hold their breath. High-resolution MRI acquisition in the free-breathing state is of high clinical relevance, as hemodynamic parameters may differ between breath holding and free breathing. At high ($\geq$3 T) and ultrahigh magnetic fields ($\geq$7 T), ECG triggering is additionally hampered by the corruption of the ECG due to the magnetohydrodynamic (MHD) effect (see Fig. 1).[2]

The MHD effect generates potential differences, mainly related to aortic blood flow, which represents a conducting fluid displaced in a strong static magnetic field. These potential differences superimpose on the potentials measured by the electrocardiogram used for gating during cardiac magnetic resonance imaging (Fig. 1).

A radio detection and ranging (radar) sensor is based on the detection or measurement of the microwaves reflected

[a]Electronic mail: florian.thiel@ptb.de.

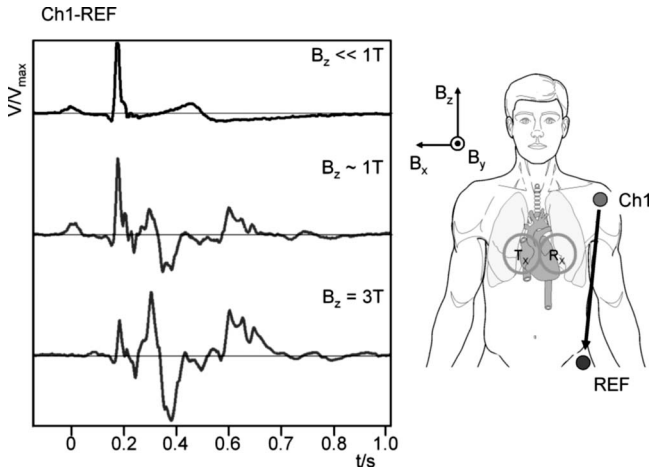

FIG. 1. Left: corruption of the ECG (Einthoven III) due to the MHD effect in different static magnetic fields (mean of 30 ECGs of a healthy volunteer). Right: electrode position for the ECG and orientation in the static field ($B_x, B_y \ll B_z$).

from an object after short-range free-space propagation. Using broadband signals offers the advantage to gain more object information rather than utilizing a single frequency (e.g., Doppler radar),[3] i.e., observation of the change in material characteristics over a wider frequency range under a certain physical or chemical influence. Furthermore, from basic system theory follows that exposing an object to UWB signals (0.1–10 GHz) gives access to its impulse response function (IRF), i.e., the frequency response function, due to their noise like behavior.[4] The IRF contains not only information on the surface of the object but also of its internal structure, since the objects' radar cross-section depends on the reflection coefficient which itself depends on the internal composition of the object,[5] whereas the low-frequency components pronounce the deeper structures of the object and the high frequency components pronounce the surface structure due to their lower penetration depth. UWB electromagnetic excitation signals, e.g., pulses or pseudonoise (PN) (covering a spectral bandwidth up to 10 GHz), generated by an UWB radar and transmitted by an appropriate antenna,[6] are able to probe the human body with low integral power (~1 mW) because electromagnetic waves can propagate through the body and are reflected at interfaces between materials of different dielectric properties, e.g., muscle/adipose tissue interface. The reflective response varies according to the displacements of the individual interfaces.[7]

Therefore, we proposed the application of a combined MRI/UWB radar technique for a contactless, noninvasive monitoring of the positions of the heart muscle and the chest. This approach is not affected by the strong static magnetic fields and field gradients of a MR scanner and reproduces the displacement of stratified biological objects with high accuracy, which we have evaluated on tissue mimicking phantoms and *in vivo* on a recently developed MR/UWB radar prototype.[8] The UWB device used in this study generates signals covering the frequency band from dc to 5 GHz. The UWB antennas applied reduce this frequency range down to the range from 1 to 5 GHz due to their high pass properties.[6] The signal-to-noise (SNR) of a MR scan is not affected by the UWB signals, since the receiver bandwidth of 10–100 kHz is very low compared to the gigahertz bandwidth of the UWB system. Moreover the antennas attenuate the transmitted UWB signal at 125 MHz, the Larmor frequency of protons at 3 T, by more than 100 dB. Comparing MR images taken from a MR head phantom with and without UWB exposure, within measuring uncertainty, no additional noise could be observed. So, according to expectation, the MRI system was not affected by the UWB signals, as these appear as a low power noise source to the MR system.

To execute MRI in a predefined state of the heart cycle (e.g., end-systolic, end-diastolic, or in a chosen intermediate state), the definition of landmarks in the acquired UWB signatures, which offer a mechanical representation of the electrically activated myocardium, is demanded for controlled MRI data acquisition. For this purpose, analysis and interpretation of physiological signals acquired by UWB radar are essential. These cardiac mechanical signals must be interpreted by comparison with established techniques; those in relation to the global myocardial mechanics are well established in clinical praxis, e.g., high-resolution ECG. Only in this way a sound understanding of the myocardial mechanics rendered by biomedical UWB radar monitoring can be gained. The interrelation between the electrical and mechanical activity of the human heart is known to be strong and very well-investigated using the ECG together with other methods, e.g., ultrasound or invasive catheter-based methods.[9,10] Based on this knowledge, all standard epochs (PQ, QRS, QT, etc.) in the ECG are closely related to mechanical activity of different functional parts of the heart, e.g., contraction and relaxation of the atria or the ventricles or opening of the different types of valves connecting the functional units. Additionally, the relation between pressure, volume, and flow in the individual units is also well known for each cardiac compartment.[11,12] There are also well-established MRI methods evaluating ventricular deformation, but these techniques focus on a selected slice or part of a cardiac compartment.[13] Thus, these methods are more suitable if reflections of a restricted myocardial area focused by an antenna array should be compared to the real displacement of this part.

Several attempts have been made in the past to show the interrelation of reflected microwave signals from the human thorax and simultaneously acquired ECG data, e.g., Refs. 3 and 14. These studies restricted their investigation on analysis of overall correlation between the two modalities or focuses on the detection of heart rate variability by the applied radar method focusing on surface displacement.[15,16] Other contributions avoid the problem of microwave signal damping and dispersion while propagating through the different tissues of the thorax by an unphysiological *ex vivo* investigation of excised hearts.[17] Unfortunately none of those carried out an in-depth interpretation of the correspondence between the different ECG episodes and the mechanical data, which is the prerequisite for understanding and in our case the basis to identify landmarks for triggering a magnetic resonance scanner. Even one of the latest publications related to this topic[18] concludes that the community is still in need

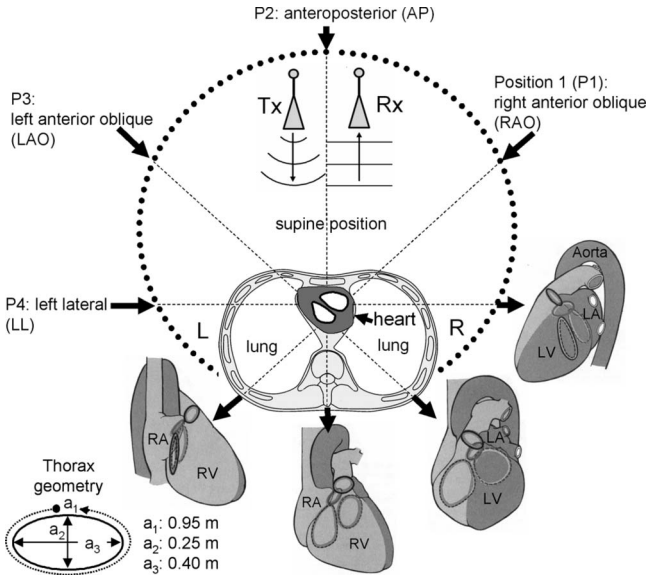

FIG. 2. Radiographic standard positions (positions 1–4) and the corresponding part of the myocardial surface mainly exposed to the UWB electromagnetic signal; anatomic pictures taken from Ref. 11; anatomical sketch for orientation and height of the eighth segment of the thoracic spine, Th8; view from the subject's head toward the feed. RA/LA: right/left atrium, RV/LV: right/left ventricle. Lower left: approximated thorax geometry of the volunteer.

of further interpretations of the electromechanical coupling presented by an ECG/microwave approach.

This article proposes an experimental setup and deals with the interpretation of signals reconstructed from UWB radar measurements if the myocardial muscle is illuminated from different well-selected spatial directions and in different respiratory states. The analysis is based upon the comparison with simultaneously acquired ECG signals and a physiological interpretation is given by epoch comparison with mechanical reference data taken from the literature. The analysis is carried out for surface reflection data and for reflections from strong reflective interfaces in the depth of the thorax, i.e., the myocardial surface. The measurement protocol had been approved by the local ethics committee and written informed consent was obtained from each participant according to the Declaration of Helsinki.

II. METHODOLOGY

The contraction of the heart, which is embedded in the chest closely behind the sternum, is a complex three-dimensional movement. Therefore, it can be concluded that illumination with electromagnetic fields from different directions will result in distinguishable contraction patterns. In this way, one can potentially monitor different parts of the myocardial surface, which are closely coupled to different cardial functional units (compartments), exhibiting its own spatiotemporal form of contraction (e.g., right/left ventricles, right/left atria, aorta, apex, etc.) (see Fig. 2). The variance (reproducibility) of myocardial contraction is known to be high (poor), hence the spatial position of each compartment varies considerably between consecutive contractions. To exploit the capabilities of new high-resolution imaging techniques, e.g., MRI at 7 T and above, this fact has to be considered.

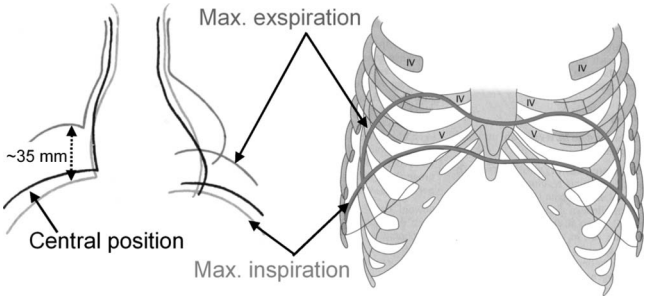

FIG. 3. Position of the diaphragm and the rips (right) and corresponding contour of the heart (left), which is attached to the diaphragm, in different respiratory states (ME and MI); anatomic sketches taken and adapted from Ref. 12.

To investigate the capabilities of a noise radar technique to monitor the cardiac compartments' individual spatiotemporal form of contraction and to maintain comparability with clinical convention, we selected the electromagnetic illumination from radiographic standard positions[11] as indicated by Fig. 2. To exclude the superimposed effect of breathing, which would otherwise dominate the UWB signal, in this part of the investigation the subject is asked to hold breath. By doing so it has to be considered that the heart muscle, which is attached to the diaphragm, changes its static shape according to the amount of air volume the lungs contain, e.g., in a state of maximal inspiration (MI) or of maximal expiration (ME) (Fig. 3). The changed cardiac contour will surely affect the radar cross-section. Hence, an investigation of the differences in the UWB signals caused by the selected respiratory states is also required. Spontaneous breathing slightly displaces the diaphragm around the central position of the diaphragm and the state of maximum inspiration lies close by, as indicated in Fig. 3. The maximal expirated state can be considered as an extreme case which changes the heart's contour significantly (Fig. 3). Furthermore, this state will change the haemodynamic parameters very rapidly due to the fast decrease/increase in oxygen/carbon dioxide level (homeostasis), which is rendered by deviation from the normal ECG form. Hence, this state of breath hold is not favorable for cardiac investigations. To this end, we started our investigations in the maximum inspirited state (MI). The maximal expirated (ME) state is examined together with the results given by the spontaneous breathing state (NA).

III. EXPERIMENTAL SETUP

In the following, the setup for the simultaneous monitoring is described. A spontaneously breathing volunteer was positioned in supine position underneath an arched antenna fixture (according to Fig. 4), where our MR-compatible tapered slot UWB antennas (T_x/R_x) (Vivaldi type)[6] are positioned in a bistatic arrangement about 120 mm above the sternum in all four positions as indicated in Fig. 2. The ambient conditions inside a MR scanner are defined by three types of magnetic fields. A static magnetic field B_{stat} of order of a few Teslas aligns the proton spins of the regions under

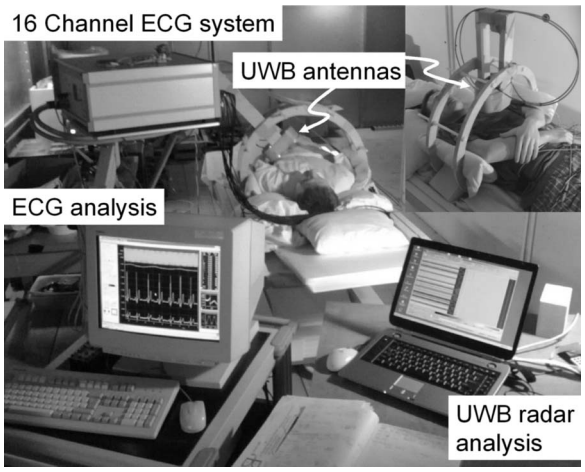

FIG. 4. Setup for the simultaneous acquisition of the electrocardiogram and the reflected UWB signals. The inset presents a closer view of the bistatic antenna arrangement above the chest of the volunteer.

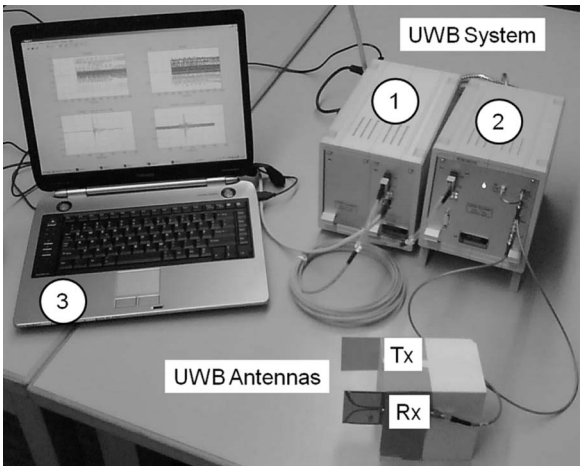

FIG. 5. Prototype of our MR-compatible UWB system (MEODAT GmbH, Ilmenau, Germany), designed according to the Medical Device Directive, in a basic setup of for UWB measurements; 1: galvanic isolation, 2: M-sequence baseband module (0–5 GHz). 3. Controlling PC and analysis software. T_x/R_x: transmitting/receiving antenna.

inspection. For diagnostic measurements, gradient fields are switched with a rise time of $dB_{\mathrm{grad}}/dt=50$ T/s to provide tomographic molecular spectra. Eddy currents are induced in the metallized sections of the antenna which, in turn, interact with the static field by exerting a mechanical torque. Therefore the design of MR-compatible UWB antennas has to consider several criteria: (1) weakly frequency dependent radiation patterns over the entire bandwidth; (2) lower cutoff frequency around 1 GHz; (3) minimized contiguous metallized areas to minimize low-frequency current loops; and (4) good decoupling between neighboring antenna elements for bistatic radar arrangements.

A. Characteristics of Physikalisch-Technische Bundesanstalt's (PTB's) reference ECG system

The ECG was obtained using a noncommercial, PTB prototype reference recorder with the following specifications: (i) resolution: 16 bit with 0.5 μV/LSB (2000 A/D units per millivolt); (ii) bandwidth: 0–1 kHz (synchronous sampling of all 16 channels); (iii) noise voltage: maximum 10 μV (pp), respectively, 3 μV (rms) with input short circuited. The data acquisition of the ECG system and the UWB radar is synchronized by a trigger signal provided by the UWB radar indicating the start of each individual measurement. To suppress interfering signals, the measurements were performed in the radio frequency (RF) shielding of PTB's Berlin magnetically shielded room 2 (Refs. 19 and 20) (Fig. 4). The high resolution and virtual elimination of interfering external signals reduces ambiguity to a minimum level. Although this is a laboratory setup to maximize SNR, it is also applicable in clinical settings, outside the shielded room.

The ECG electrodes were positioned according to DIN EN 60601-2-51 (right shoulder, left shoulder, left hip, representing the Einthoven I, II, III lead systems).

Additionally, a breathing sensor (strain gauge) was placed in the umbilical region (lower stomach). Prior to the final measurements, a test ECG was recorded from the volunteer to check for healthiness by using an ECG database. An automatic analysis of ECGs had been developed, based on the comparison with an ECG database comprising more than 10 000 ECGs.[21–23] The ECGs were collected from healthy volunteers and patients with different heart diseases and were interpreted by cardiologists of Charité-Universitätsmedizin Berlin. The analysis confirms the normality of the subject's test ECG. Nonetheless, a certain tendency toward an incomplete right bundle branch block (second grade) was also identified, indicated by the double peaks at the end of the QRS complex (see ECGs in Fig. 9 at time position S). This tendency might result in a decreased contraction delay between the right and the left ventricles.

B. Characteristics of UWB radar

The applied prototype of our MR-compatible UWB system (MEODAT GmbH, Ilmenau, Germany), designed according to the Medical Device Directive, comprising galvanic isolation, M-Sequence baseband module (0–5 GHz), controlling personal computer (PC) with analysis software, and UWB antennas in a bistatic arrangement are depicted in Fig. 5.

The goal of UWB radar is to obtain the IRF of a certain object under test (Fig. 6). The quality of a measured IRF is mainly determined by the ability to separate closely located peaks and to avoid the masking of smaller peaks due to noise or saturation effects caused by larger signals (Fig. 7 upper time course). The classical UWB approach is based on impulse excitation, which implies that the whole transmission chain is subjected to high peak power. In order to stress the electronics evenly, it is preferable to use continuous wideband signals due to the reduced crest factor. Typical examples of such signals are swept or stepped sine waves, random noise,[25] or PN sequences. However, this kind of target stimulation will not provide the IRF directly. It rather requires an appropriate impulse compression technique (i.e., Fourier transform, correlation, or matched filtering), which is often the challenge for the different system concepts. Also, after impulse compression, the flat spectral energy distribution of the signals is lost. Thus, the best one can do is to

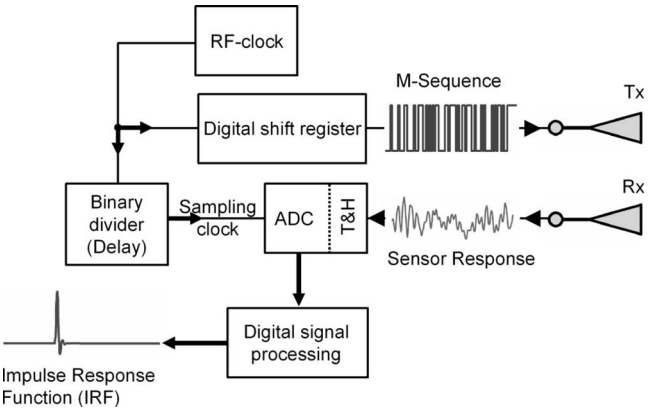

FIG. 6. Basic structure of the maximum length binary sequence (M-sequence) measurement head in block schematics (Ref. 24). T&H: Track and hold circuit. T_x, R_x: transmit and receive antenna.

carry out impulse compression in the digital domain. The digital dynamic range is only limited by the utilized data format, which can usually be selected freely. A UWB concept dealing with continuous wave excitation, a largely reduced analog circuit part, and a minimum of components was first introduced in 1999.[26] It provides maximum length binary sequence (M-sequence) signals to stimulate the test objects, which optimize the crest factor and therefore solve the overload and saturation problem. This original approach forms the basis for different extensions and improvements. The basic structure of such an UWB radar module is described below.

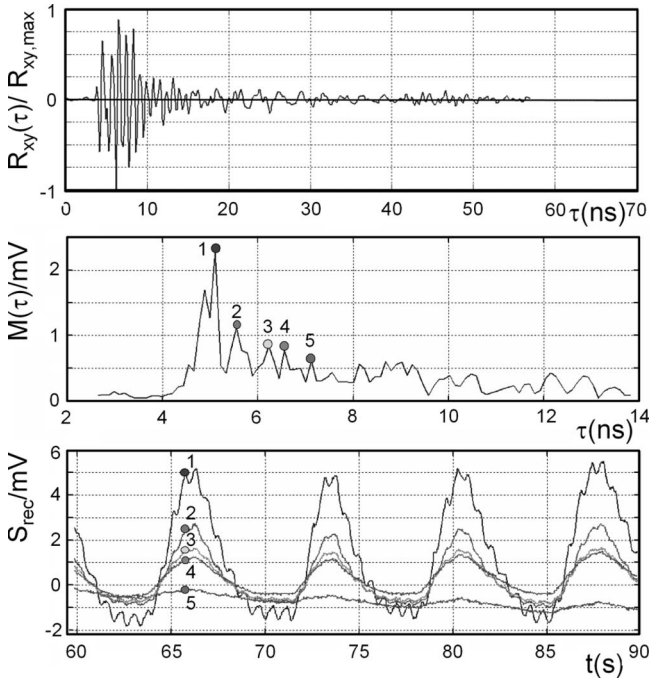

FIG. 7. The resulting reflected UWB signal is a superposition of multiple reflections. Upper graph: mean cross-correlation data $R_{xy}(\tau)$ from the transmitted and received signals provide information of the propagation time τ necessary for the electromagnetic pulse to reach an interface. Measured physiological signatures using the proposed algorithm. Middle graph: $M(\tau)$. Lower graph: time courses S_{rec} corresponding to the labeled local maxima of $M(\tau)$. Data from a normal breathing subject.

C. The *M*-sequence approach to UWB applications

The basic idea of a maximum length binary sequence (M-sequence) device initially intended for baseband operations at, e.g., 0–5 GHz is known from a couple of former publications (see Refs. 24 and 27) and the theory of pseudorandom codes and their application is given in, e.g., Ref. 28, in an introductory form. The basic structure of a wideband M-sequence device is presented in Fig. 5. The M-sequence—the stimulus signal for the object to be investigated—is generated by a digital shift register which is addressed by a stable RF clock with frequency f_c. The capturing of the measurement signal is accomplished by using a subsampling approach. One of the most important features of the M-sequence approach is that the actual sampling rate f_s can be derived in a simple and stable way (i.e., by a binary divider) from the RF master clock such that $f_c=2^n f_s$ (see Fig. 6 and Ref. 27 for details).

Time-domain measurements use correlation processing in order to gain the wanted IRF of the material under test. In that case, unwanted external narrow band perturbations will be spread over time, since they are not correlated with the test signal. In this way, they cause the same effect as white noise, which is often less critical than a corruption of the whole waveform in time-domain in the case of a classical time-domain reflectrometry analysis, or the strong perturbation of individual frequency bands in the case of network analysis.

IV. SIGNAL PROCESSING AND DATA ANALYSIS

To extract displacements from interfaces built from various biological tissues out of reflected broadband microwave signals, appropriate algorithms have to be developed and tested. These algorithms are crucial to identify relevant signals in static and dynamic multipath reflections (clutter), as well as to decompose significant physiological signatures from the multiple superimposed impulse responses generated by the object under test. Our algorithms are based on an analysis of eigenvalues, extracted from the covariance matrix Q calculated from the cross-correlation data $R_{xy}(\tau)$ of the transmitted and received signals. $R_{xy}(\tau)$ is provided by the UWB controller where each of the N rows is an observation containing M samples, and each of the M columns represent a time shift $\Delta\tau$ (Fig. 7, upper part). If we define the rows of R_{xy} to correspond to all measurements of a particular type and each column to a set of measurements from one particular trial, the covariance matrix becomes $Q=1/(N-1)\,R_{xy}R^T_{xy}$. Q captures the correlation between all pairs of measurements. The covariance measures the degree of the linear relationship between two variables, where a large (small) value indicates high (low) redundancy. The main diagonal elements $\lambda_Q=\{\lambda_{Q,11},\ldots,\lambda_{Q,MM}\}$ of Q are the variance of particular measurement types and the off-diagonal terms are the covariance between measurement types indicating redundancy. In the diagonal terms the interesting dynamic is reflected. Given that, we ignore redundancy information by setting the off-diagonal terms to zero, which results in a diagonal matrix D

$$D=\mathrm{diag}(\lambda_Q). \tag{1}$$

Therefore λ_Q contains the eigenvalues of the diagonal matrix D for each time shift τ, which is an estimate of the momentary signal variance. Each eigenvalue corresponds to a certain time shift τ

$$M(\tau) = \lambda_Q(\tau). \tag{2}$$

$M(\tau)$ displays the signal variance at each propagation time (Fig. 7, middle). Thus, significant values in $M(\tau)$ correspond to relevant interfaces (which have a large reflection coefficient), which are displaced by physiological events. This means that interfaces exhibiting high dielectric contrast, e.g., a fat/muscle interface, produce large reflections, i.e., a large peak with a steep slope in the IRF at the propagation time which corresponds to this interface. Hence, small displacements of this IRF creates a large signal at the position of the slope and our algorithm searches for these propagation times, because $M(\tau)$ displays the signal variance at each propagation time. According to the analysis at a fixed propagation time τ we call this approach "τ-locked" analysis. The interfaces which we state as "relevant" are such high contrast interfaces such as the air/skin interface and the fat/pericardium/myocardium interface.

We have tested this algorithm with synthetic physiological signals, generated applying an analytical thorax model, and found good agreement between the reference time course and the reconstructed motion.[7] We found the absolute deviation from the maximal reference amplitude to be smaller than 2% and is caused by the nonlinearity of the transfer function introduced by the algorithm.[7] Since our transfer function is formed from the flange of a certain interface reflection in the IRF, its linearity is only guaranteed for small displacements like those we expect by respiratory and myocardial events. The deeper the interesting interface is located in the depth of the body, the flatter becomes the transfer function due to dispersive effects, i.e., the sensitivity decreases. For this algorithm we calculated a theoretical deviation which is equivalent to a reconstruction uncertainty of 100 μm.[7]

To affirm the validity of our algorithm it was also tested on phantoms closely mimicking the layered tissue arrangement of the human thorax, which were moved in a controlled way with high spatial precision.[29] Furthermore, the algorithm was tested on a volunteer mimicking the envisaged biomedical applications simultaneously with magnetic resonance imaging.[30] These tests, particularly aiming to reproduce a breathing paradigm and the superimposed cardiac contraction, exhibit good correspondence between calculated time courses and physiological reality. The tests proved the ability of the algorithm to detect movements in the submillimeter range even for harsh experimental conditions.

In the first step of our combined ECG/UWB radar experiment we were interested in the displacement of the thoracic surface detected from different illumination positions according to Fig. 2. In a second step the propagation time interval in $R_{xy}(\tau)$, representing the surface displacement, was excluded from the analysis and the reflection signal of the next high reflective interface was analyzed. By assuming a mean value for the dielectric constant the depth of this interface can be estimated. According to the dispersive behavior of biological tissue, the signal from deeper interfaces should be smaller in amplitude and resolution should be reduced, which reduces the sensitivity to small variations and smoothens fast transitions. For an analysis of deeper interfaces, appropriate deconvolution techniques must be applied if significant ringing in the IRF of the antenna occurs (e.g., adapted Wiener method). The applied antennas exhibit negligible ringing,[6] so the influence of antenna's IRF can be considered to be marginal.

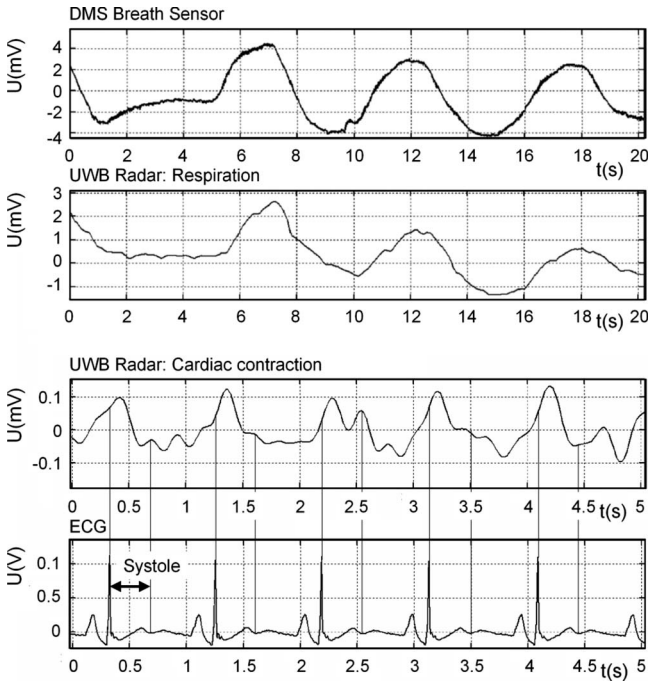

FIG. 8. Upper two time courses: comparison of the time courses measured by the breath sensor located at the umbilical region and the signals extracted from the UWB radar data at the height of Th8. The two lower time courses presents the UWB signal in a breath hold (MI) and the corresponding high-pass filtered ECG (EII) (lowest). The connecting lines indicate the systolic phase (contraction).

Prototypical measurements are given in Fig. 8, the respiratory signal extracted from $R_{xy}(\tau)$ applying the proposed algorithm is juxtaposed to the simultaneously acquired signal from the applied breathing sensor (Fig. 8, upper two time courses). The slight phase shift in the reconstructed breathing signal is caused by the different acquisition positions of the two sensors (UWB antennas located at the sternum, the strain gauge in the umbilical region, i.e., below the stomach). The lower part of Fig. 8 offers the juxtaposition of the extracted UWB signatures representing cardiac motion, and the corresponding ECG. The mechanical myocardial signals we reconstructed from a breath hold can be regarded to be entirely of myocardial origin.

For further analysis we extracted and clustered (overlapped) the ECGs of each measurement (~40 s) and did the same for the corresponding epoch in the reconstructed UWB time courses (Figs. 8 and 9).

V. INVESTIGATION OF SURFACE REFLECTIONS

If an electromagnetic wave propagates through a stratified dielectric medium, it suffers from dispersion and damping. Thus, with increasing penetration depth high frequency

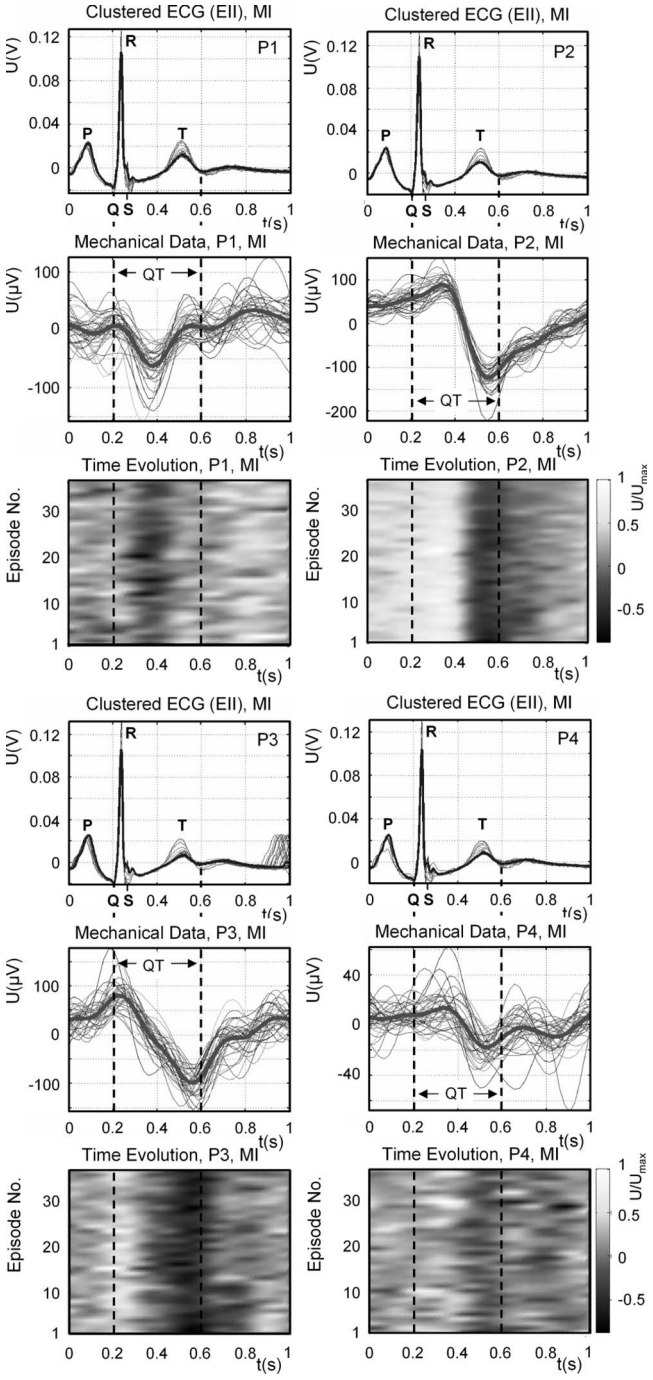

FIG. 9. Evolution of the reconstructed surface displacement intervals measured in a breath hold (MI) in the four selected positions. The overlapped ECG intervals and its mean value (bold gray line) and the corresponding overlapped epochs form the reconstructed mechanical time course and its mean value (bold gray line) is juxtapositioned for all four illumination positions P1–P4. Additionally the juxtaposition of the time evolution of the mechanical epochs for each position is added to give more information about the variation in the mechanical data.

components are significantly attenuated. Therefore we expect the surface reflection signals to be the strongest and the one with best spatial resolution. It is well known that the complex three-dimensional deformation of the heart displaces the thorax's surface locally by an amplitude of ~1 mm at the fifth spatium intercostale (apex beat).[31] The fifth spatium intercostale is illuminated in positions 2 and 3. Therefore, we expect the largest signal at these illumination positions.

Figure 9 comprises typical results of our signal processing procedure for surface reflection date located at the absolute maximum of $M(\tau)$. Comparing the time courses in Fig. 9, it becomes obvious that the global variance of the clustered, extracted signals varies remarkably between the electrical activation and the mechanical response, displayed by UWB radar. This is in good agreement with the experiences from clinical ultrasound investigations of cardiac contractility variability, and indicates that the myocardial activity is not only controlled by the electrical excitation, but is part of other physiological control loops using different metabolic factors (e.g., hormonal, oxygen level, etc.).

However, it is interesting to note that the increased local variance in the ECG seams to be very well reflected by an increased variance in the corresponding reconstructed mechanical signals at later times in close proximity (see especially the T position for P2 and P3 in Fig. 9). This retardation is physiological, for each mechanical activity is preceded by the electrical polarization/depolarization of the myocardium (Fig. 12).

VI. INVESTIGATION OF SUBSURFACE REFLECTIONS

To investigate how the surface reflection representation renders the complex three-dimensional intrathoracic deformation of the myocardium in a breath hold, subsurface reflections have to be analyzed. From our modeling,[7] amplitude reduction is expected as well as significant damping of high frequency components which will result in the loss of spatial resolution. We do not consider refraction in this study.

To gain such signals the following procedure was applied. In our search in $M(\tau)$ for significant interfaces the propagation times corresponding to the surface reflection were ignored, and the search was proceeded starting at a later (approximately penetration depth) position. The spatial resolution in a certain medium is defined by the dielectric properties of the medium and the sampling time $\Delta\tau$ defined by the UWB device's hardware, which in our case is around $\Delta\tau \approx 111$ ps. In air, where the mean real part of the permittivity ε' equal unity, this is equivalent to the resolution of a propagation length of approximately $\Delta s \approx 3$ cm.

To give an estimate of the propagation depth s^* below the surface, where the new interface is identified by our τ-locked algorithm, we have to assume a mean real part ε' of the permittivity for each illumination position in the frequency range from 1–5 GHz, for s^* is proportional to the propagation time τ_M times the propagation velocity $c = c_0/\sqrt{\varepsilon'}$ in this medium (c_0 is the propagation velocity in free space, i.e., $\varepsilon'=1$). The values for ε' were taken from Ref. 32. Since the propagation way for positions 1 and 3 is a mixture of tissue with high and low water content ($\varepsilon'_{\text{Muscle}} \sim 60$) and lung tissue ($\varepsilon'_{\text{Lung}} \sim 20$) we can assume $\varepsilon'_{1/3} \sim 50$, giving an estimate for the propagation depth to reach the next relevant interface $s^*_1 = 5.6$ cm (resolution per sample $\Delta s^*_1 = c_0 \Delta\tau/\sqrt{\varepsilon'} = 0.46$ cm), $s^*_3 = 4.6$ cm ($\Delta s^*_3 = 0.46$ cm) (see Fig. 2). For position 4 we assume $\varepsilon'_4 = 30$ due to its long passage through lung tissue ($\varepsilon'_{\text{Lung}} \sim 20$). This results in a propagation depth of $s^*_4 = 11.4$ cm ($\Delta s^*_4 = 0.6$ cm). The dielectric constant for the propagation way given by position 2

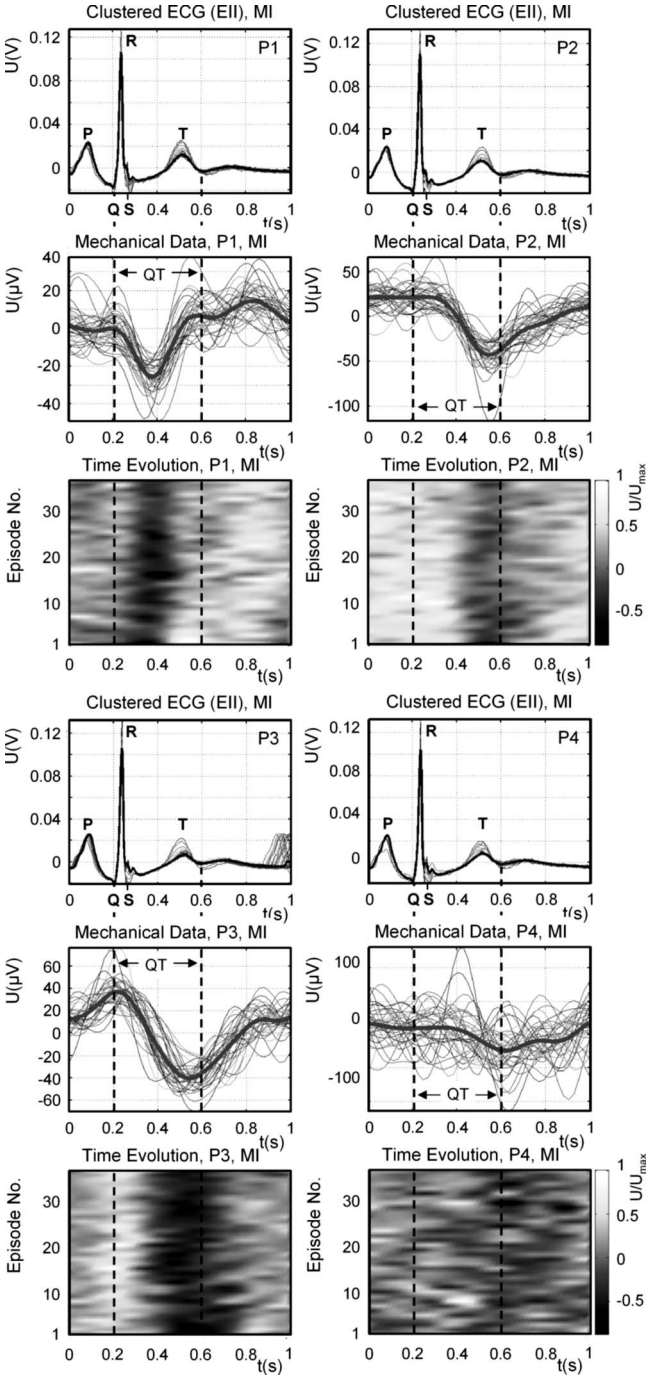

FIG. 10. Evolution of the reconstructed subsurface displacement intervals measured in a breath hold (MI) in the four selected positions. The overlapped ECG intervals and its mean value (bold gray line) and the corresponding overlapped epochs form the reconstructed mechanical time course and its mean value (bold gray line) is juxtapositioned for all four illumination positions P1–P4. Approximated linear propagation path length behind the thorax surface: P1: $s^*_1=5.6$ cm ($\varepsilon_1'\sim 50$, $\Delta s^*_1=0.46$ cm), P2: $s^*_2=5.1$ cm ($\varepsilon_2'\sim 60$, $\Delta s^*_2=0.42$ cm), P3: $s^*_3=4.6$ cm ($\varepsilon_3'\sim 50$, $\Delta s^*_3=0.46$ cm), P4: $s^*_4=11.4$ cm ($\varepsilon_4'\sim 30$, $\Delta s^*_4=0.6$ cm). Additionally the juxtaposition of the time evolution of the mechanical epochs for each position is added to give more information about the variation in the mechanical data.

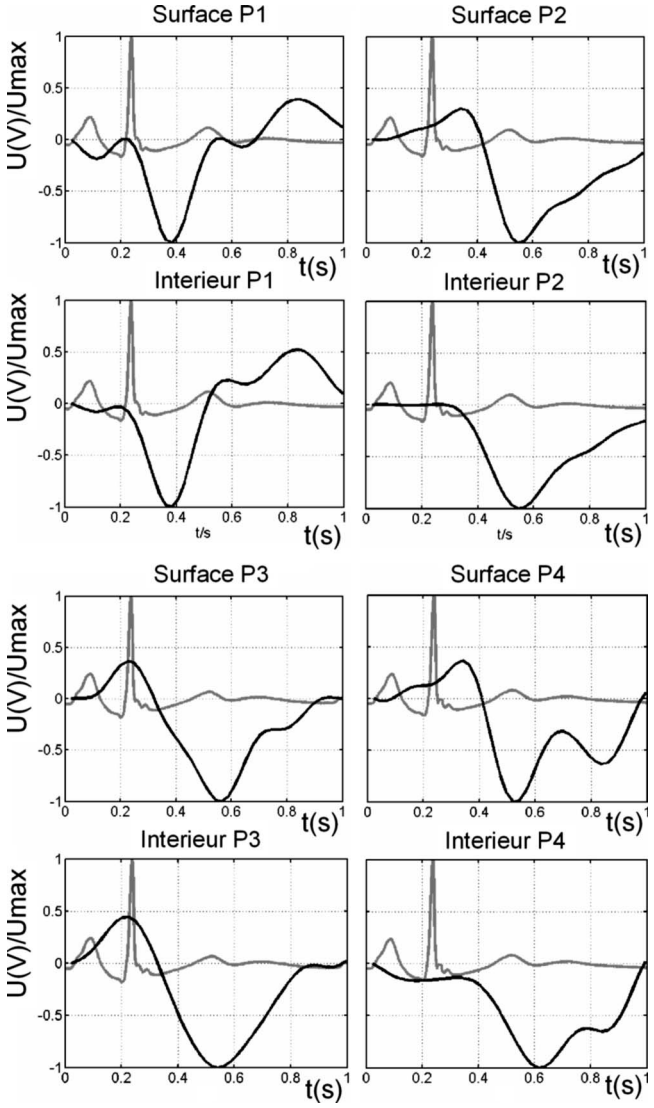

FIG. 11. Comparison of the mean mechanical data juxtapositioned with the corresponding ECG of the surface and subsurface reconstruction for all four illumination positions. Approximated linear propagation path length behind the thorax surface: P1: $s^*_1=0.056$ m, P2: $s^*_2=0.051$ m, P3: $s^*_3=0.046$ m, P4: $s^*_4=0.114$ m.

will be highest, $\varepsilon_2'=60$ because of the high water content tissue (muscle) in the propagation way, giving $s^*_2=5.1$ cm ($\Delta s^*_2=0.42$ cm).

As expected, the subsurface interface where the new mechanical representation from the individual illumination position comes from, is very similar for positions 1, 2, and 3. The propagation path is slightly shorter for position 3, which could also be expected since the heart is located between the lungs in the middle of the chest, behind and slightly to the left of the thorax's breastbone (sternum). Also, according to expectations, the propagation depth for position four is the deepest. Assuming negligible mean refraction due to the propagation through the sequence of dielectric layers with varying properties (linear propagation path) it is also interesting to note, that all propagation lengths are in good agreement with the volunteer's thoracic geometry, which we can approximate by an infinite long elliptic cylinder with circumference $a_1=0.95$ m, major axis $a_2=0.4$ m, and minor axis $a_3=0.24$ m as indicated in Fig. 2. A comparison of the mechanical signals from the surface and the intrathoracic interface is given in Fig. 11. According to expectation, small variations cannot be resolved (see Fig. 11). Furthermore in

all illumination positions the strongest variation, which is related to the systolic contraction of the ventricles is broadened which is an indicator for the dispersive behavior of the stratified dielectric object. Generally we can conclude that the surface signal closely approximates the subsurface reflections.

VII. RESULTS

A. Mechanical representations during a breath hold from four different illumination positions

To evaluate the surface UWB time courses, a standard Wiggers diagram (WD),[11] comprising the pressure in the different cardiac functional units in marked contraction phases, is juxtaposed to the recorded ECG epochs (Fig. 12). As expected, the mechanical representation varies depending on the illuminated superficial part of the myocardium. Nevertheless, similarities can be identified. Most eye-catching is the strong change in signals in the course of the systolic phase (start at 1, end at 3 in the WD, Fig. 12, QT interval in the ECG, Fig. 9). Due to the contraction of the myocardium (~−25% of diameter), the radar cross-section decreases accordingly. Additionally, the contraction pattern of different functional units can be distinguished by examination the different illumination directions, e.g., the extreme cases of P1 and P4. For instance, the contraction of the right/left atrium (see Fig. 12, A/A^*), the contraction of the right/left ventricle (Fig. 12, B/B^*) and the filling of the right/left ventricle (Fig. 12, C/C^*) can be distinguished from the two positions P1 (RAO) and P4 (LL). The coarse physiological temporal evolution of the cardiac cycle is as follows: (i) contraction of the right atrium, (ii) contraction of the left atrium, (iii) contraction of the right ventricle, (iv) contraction of the left ventricle, and (v) filling of the ventricle. Therefore, the delayed contraction of the left functional units with respect to the right one is rendered correctly (Fig. 12, A/A^*, B/B^*, and C/C^*). We can conclude that UWB radar is capable to trigger the MR data acquisition in these phases.

B. Mechanical representation in different respiratory states

In a second step we measured the UWB signals and the ECG in MI (Fig. 13, upper part), ME (Fig. 13, middle part) and during spontaneous breathing (NA) (Fig. 13, lower part), respectively, in all four radiographic positions (P1–P4). As expected, the mechanical representation varies with the cardiac contour and the illuminated superficial part of the myocardium.

The composition of the surface breathing signal and cardiac signal is decomposed by applying high order infinite impulse response filter (respiratory signal: cutoff frequency 0.4 Hz, cardiac signal: 0.7 Hz$<f<$5 Hz).

Due to the reduced epoch length in the ME state and in order to maintain comparability to MI and NA we reduced the over all epoch length to the length of ME in Fig. 13. Beside the mean time course in the ME state for position 4, the maximum variation corresponding to the systolic ventricular phase can be identified.

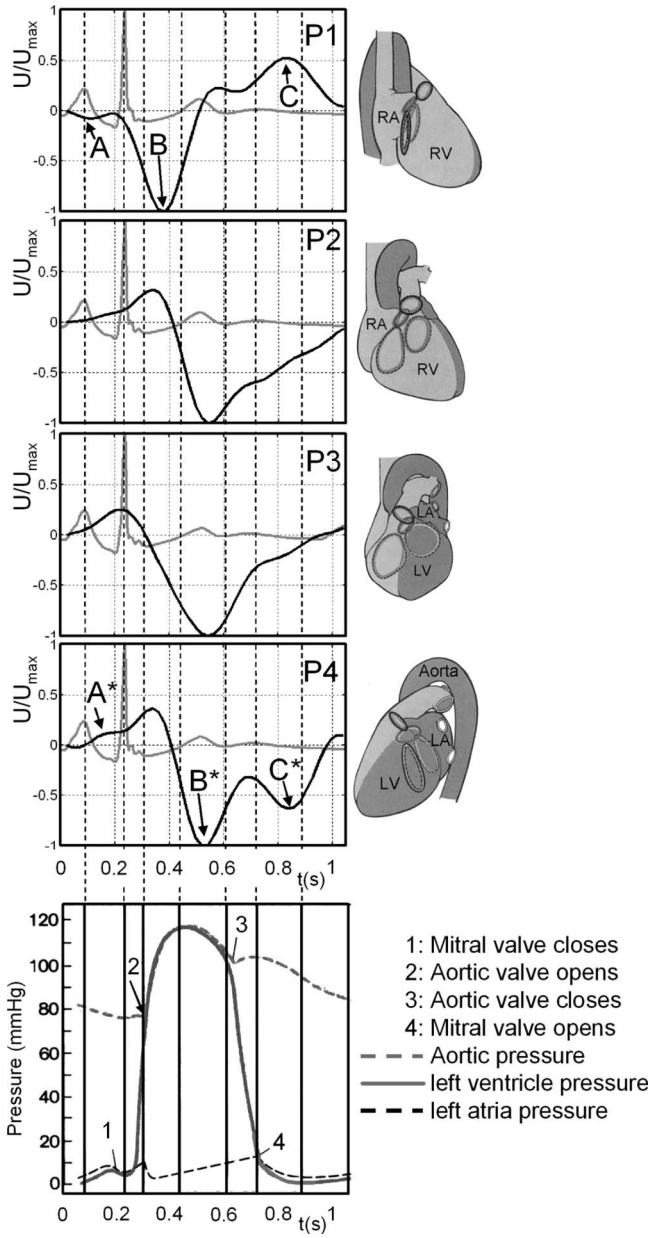

FIG. 12. Comparison of the normalized time courses reconstructed from the four exposure positions (P1, P2, P3, P4) measured during MI and corresponding ECG. The lowest time course is a part of a WD comprising the pressure in the left ventricle (bold line), the aortic pressure (dashed bold line), and the pressure in the left atria (thin dashed line). 1: Mitral valve closes (stops filling of left ventricle), 2: aortic valve opens (left ventricular volume is ejected), 3: aortic valve closes, 4: Mitral valve opens (filling of left ventricle). Anatomical pictures and pressure curve taken and adapted from Ref. 11. A/A^*: contraction of right/left atrium. B/B^*: contraction of right/left ventricle. C/C^*: filling of right/left ventricle.

In the following we will apply our noninvasive monitoring of the myocardial contraction to an actual safety issue, which arose with the advent of high field (>1.5 T) magnetic resonance scanners in clinical praxis and research.

VIII. EXEMPLARY APPLICATION TO MRI SAFETY: INFLUENCE OF STRONG STATIC MAGNETIC FIELDS ON MYOCARDIAL MECHANICS

ECG is excessively used for triggering MR data acquisition to image the heart in a certain stage of contraction or

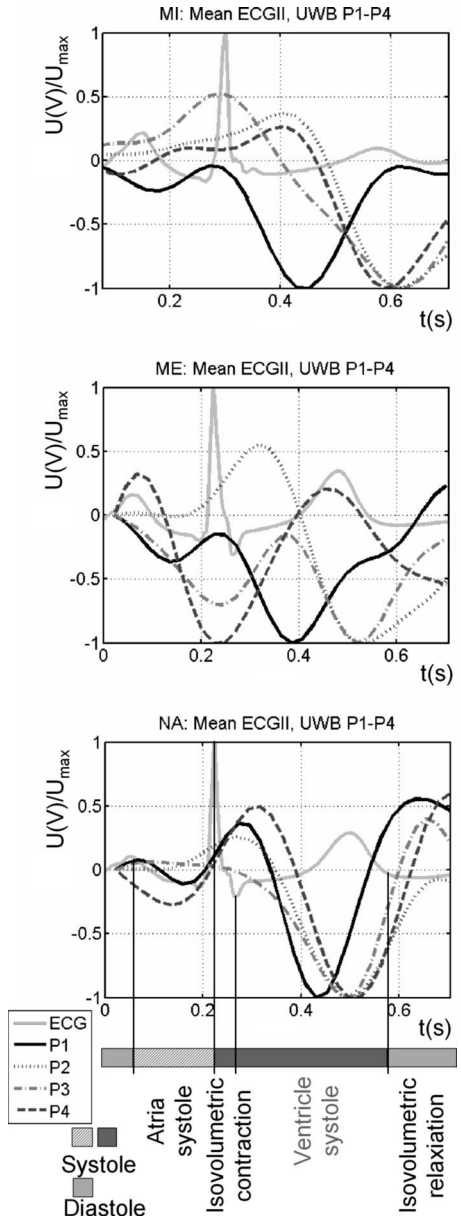

FIG. 13. Comparison of the normalized time courses $(U/U_{\max})$ reconstructed from the four radiographic standard positions measured in two static (MI/ME) and one dynamic state of respiration (NA). The ECG is included as a reference. Upper: maximum inspiration. Middle: maximum expiration. Lowest: normal spontaneous breathing.

to prevent reduction in image quality by motion artifacts generated by the strong nonlinear motion of the heart muscle. Unfortunately, there is increasing difficulty to use the ECG for MR triggering especially at B_0-fields beyond 1.5 T due to the MHD effect[2] (Fig. 1). If the conducting particles of the blood are redirected by the magnetic field, it is only consequent to ask whether the electrical excitation spread over the myocardial muscle, which is based on ionic transportation, is redirected, too. Such a redirection should be visible in the ECG and in a deviant myocardial contraction, which is directly dependent on the spatiotemporal devolution of the excitation spread. Unfortunately, investigating this effect using the ECG itself is not possible since it is dominated by the MHD effect. Thus, we propose to use UWB radar to monitor the global myocardial dynamics inside an MR scanner.

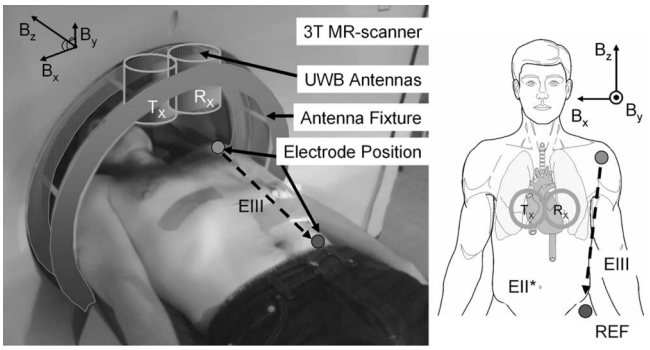

FIG. 14. Right: positioning of ECG electrodes and UWB antennas. Left: setup of the combined ECG/UWB measurement at the 1 T position just outside the bore of the 3 T scanner.

We simultaneously acquired ECG and UWB radar data: (i) at $B_0 \approx 0$ (earth's magnetic field), (ii) at $B_0 = 1$ T at the edge of the bore of a 3 T MR scanner, and (iii) at $B_0 = 3$ T in the isocenter of the scanner (see Fig. 9). A volunteer was positioned in supine position and was asked to hold his breath to exclude breathing artifacts. The MR-compatible tapered slot UWB antennas T_x/R_x (Ref. 6) were positioned about 150 mm above the sternum (position 2 according to Fig. 14) in an appropriate plane through the heart (height of the eighth segment of the thoracic spine, Th8). Position 2 was chosen due to restricted space in the MR scanner. The position of ECG electrodes and the position of the UWB antennas were not changed between the three different measurements. In Fig. 15 the median of $n=29$ ECGs, the corresponding reconstructed UWB signals representing the global cardiac dynamics and the mean sinusoidal fit of the UWB data are depicted for $B_0=0$, 1, and 3 T, respectively. To investigate, whether there is a significant change in the global myocardial mechanics between zero field and 1 or 3 T, we applied student's t-test $[t(0.95,29)$, paired, two-sided] on the UWB data for each time step in the standardized ECG epoch $t=[0,\ldots,1.1\ \text{s}]$. We found no statistically significant change among all three UWB measurements, i.e., the values of the test do not reach the limit of significance $t(0.95,29)$ indicated by the straight horizontal line in the upper right of Fig. 15. Additionally, the phase of the sinusoidal fit was compared applying a t-test $[t(0.95,29)]$ to check for excitation delays. Again, there was no significant change in phase for increasing field. We find p-values well above the significance level (see Fig. 15, lower right), represented by $\alpha = 1 - \text{erf}(n/\sqrt{2}) = 5\%$ $[p(0\ \text{T}/1\ \text{T}) \approx 0.29,\ p(0\ \text{T}/3\ \text{T}) \approx 0.66,$ and $p(1\ \text{T}/3\ \text{T}) \approx 0.62]$. Thus, we cannot reject the null hypothesis, which states there is no significant change among measurements.

IX. SUMMARY

While penetrating into the human body, the UWB signal propagates in a three-dimensional manner and reflects the motion of a large area at a certain propagation time, e.g., the surface of the heart, which follows a cyclic highly nonlinear motion. MRI is the most important tool in modern cardiology and neuroscience. Therefore, we have investigated whether UWB radar provides suitable mechanical data from

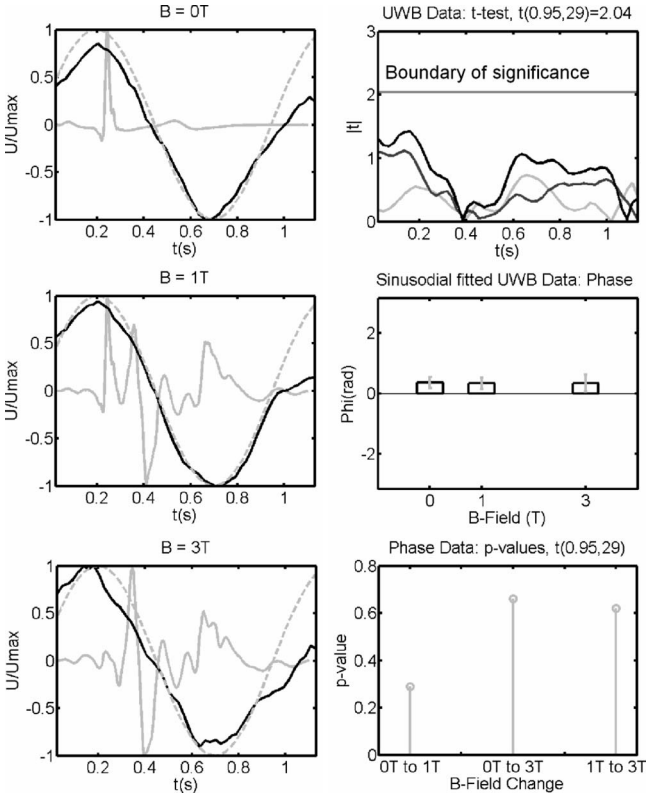

FIG. 15. Left: comparison of the median of 29 ECGs (light gray), the corresponding reconstructed mean UWB signals (black), and the mean of the sinusoidal fitted UWB data (dashed light gray) for $B_0=0$, 1, and 3 T. Upper right: result of the t-test for each time step in $t=[0,\ldots,1.1\ \mathrm{s}]$ [vertical line: $t(0.95,29)$ which indicates the boundary of significance. Other lines from highest to lowest: black line: $|t(1\ \mathrm{T}/3\ \mathrm{T})|$; light gray line: $|t(0\ \mathrm{T}/3\ \mathrm{T})|$; dark gray line: $|t(0\ \mathrm{T}/1\ \mathrm{T})|$]. Middle and lower right: comparison of phase of the fit and p-values of the t-test on the phase.

the myocardium and holds the potential to serve as a navigator technique for MRI. We have shown that the mechanical representation of the cardiac contraction provided by UWB radar varies dependent with the cardiac contour and the illuminated superficial part of the myocardium. The results are very satisfactory and prove the ability of UWB radar to monitor physiological events directly at their origin inside the body. Optimization of data acquisition by the use of UWB antenna arrays to localize the motion in a focused area, will improve the result. Possible additional applications besides the proposed MRI/UWB combination could be infarction detection, for ischemic myocardial muscle tissue results in a modified contraction pattern, potentially accessible by UWB radar. Another pathophysiological event, detectable by our technique, could be pulseless electrical activity. Pulseless electrical activity (also known by the older term electromechanical dissociation or nonperfusing rhythm) refers to any heart rhythm observed in the electrocardiogram that should be producing a pulse, but is not. The condition may or may not be caused by electromechanical dissociation. The most common causes are intoxications and hypovolemia, which is a state of decreased blood volume; more specifically, decrease in volume of blood plasma. A further application could be the identification of the mechanical equivalent to the QT interval, for recent guidelines drafts of the International Conference on Harmonization of Technical Requirements for Registration of Pharmaceuticals for Human Use (ICH) underline the necessity to test nonantiarrhythmic drugs for their potential to prolong the QT or the corrected QT interval.[33] The implementation of these guidelines requires a large amount of ECG or MCG (magnetocardiography)[34,35] measurements on animals and humans in preclinical and clinical phases of the drug development process. Therefore, we propose the use of UWB radar as a complementary method with particular advantages in high-throughput studies, where signal quality and reliability are key factors.

ACKNOWLEDGMENTS

We are grateful to A. Schnabel and F. Petsche from PTB for their help applying the ECG system. We also like to thank M.A. Hein, R. Stephan, and U. Schwarz from Technische Universität Ilmenau for providing the antennas, and to J. Sachs and M. Helbig from Technische Universität Ilmenau for their support. We would also like to thank our medical partners I. Hilger and C. Geyer at the Institute for diagnostic and interventional radiology (FSU Jena) for providing the paper work for the ethic license. This work was supported by the German Research Foundation (DFG) in the priority program UKoLoS (Grant No. SPP1202, project acronym *ultraMEDIS*).

[1] A. D. Droitcour, Ph.D. thesis, Stanford University, Stanford, Canada, 2006.
[2] G. M. Nijm S. Swiryn, A. C. Larson, and A. V. Sahakian, Comput. Cardiol. **33**, 269 (2006).
[3] H. J. Kim, K. H. Kim, Y. S. Hong, and J. J. Choi, Rev. Sci. Instrum. **78**, 104703 (2007)
[4] J. Sachs, P. Peyerl, S. Wöckel, M. Kmec, R. Hermann, and R. Zetik, Meas. Sci. Technol. **18**, 1074 (2007).
[5] B. R. Mahafza and A. Z. Elsherbeni, *Simulations for Radar System Design* (Chapman and Hall, London/CRC, New York, 2004), p. 501.
[6] U. Schwarz, F. Thiel, F. Seifert, and M. Hein, *Proceedings of the IEEE European Conference on Antennas and Propagation*, 23–27 March, 2009, Berlin, Germany (IEEE, New York, 2009), pp. 1102–1105.
[7] F. Thiel and F. Seifert, J. Appl. Phys. **105**, 044904 (2009).
[8] F. Thiel, M. Hein, U. Schwarz, J. Sachs, and F. Seifert, Rev. Sci. Instrum. **80**, 014302 (2009).
[9] T. P. Abraham, V. L. Dimaano, and H. Liang, Circulation **116**, 2597 (2007).
[10] P. Steendijk, S. A. F. Tulnera, M. Wiemerb, R. A. Bleasdalec, J. J. Baxa, E. E. van der Walla, J. Vogtb, and M. J. Schalija, Eur. Heart J. **6**, D35 (2004).
[11] C. Droste and M. von Planta, *Memorix Konstanten der Klinischen Medizin*, 3rd ed. (VCH, Germany, 1993).
[12] H. Fritsch and W. Kühnel, *Taschen Atlas der Anatomie: Innere Organe*, 8th ed., (Thieme, Germany, 2003) Vol. 2.
[13] S. Masood, G. Yang, D. J. Pennell, and D. N. Firmin, J. Magn. Reson. Imaging **12**, 873 (2000).
[14] Y. Yin, J. Qian, J. Lu, and Y. Huang, IEEE Sens. J **1**, 565 (2003).
[15] S. Hunt, A. Roseiro, and M. Siegel, *Proceedings of the Annual International Conference of the IEEE Engineering in Medicine and Biology Society*, 4–7 November 1988 (IEEE, New York, 1988), Vol. 1, p. 158.
[16] T. Matsui, I. Arai, S. Gotoh, H. Hattori, B. Takase, M. Kikuchi, and M. Ishihara, Biomed. Pharmacother **59**, S188 (2005).
[17] S. Y. Semenov, A. E. Bulyshev, V. G. Posukh, Y. E. Sizov, T. C. Williams, and A. E. Souvorov, Ann. Biomed. Eng. **31**, 262 (2003).
[18] J. Muehlsteff, J. Thijs, R. Pinter, G. Morren, and G. Muesch, *IEEE International Conference on Engineering in Medicine and Biology Society (EMBS)*, 22–26 August 2007 (IEEE, NewYork, 2007), pp. 5758–5761.
[19] J. Bork, H. D. Hahlbohm, R. Klein, and A. Schnabel, *Proceedings of the 12th International Conference on Biomagnetism*, edited by J. Nenonen, R. J. Ilmoniemi, and T. Katila, Helsinki University of Technology, Espoo, Finland, 13–17 August 2001 (Biomag, Boston 2001), pp. 970–973.

[20] F. Thiel, A. Schnabel, S. Knappe-Grüneberg, D. Stollfuß, and M. Burghoff, Rev. Sci. Instrum. **78**, 035106 (2007).
[21] R. Bousseljot and D. Kreiseler, Comput. Cardiol. **2000**, 331 (2000).
[22] R. Bousseljot, U. Grieger, D. Kreiseler, L. Schmitz, H. Koch, S. Beckmann, C. Bethge, H. von Nettelhorstt, and K. Stangl, Comput. Cardiol. **30**, 121 (2003).
[23] H. Koch, R. Bousseljot, D. Kreiseler, and L. Schmitz, The PTB Diagnostic ECG Database in PhysioBank: Physiologic Signal Archives for Biomedical Research, http://www.physionet.org/physiobank /database/ptbdb/.
[24] J. Sachs and P. Peyerl, Proceedings of the Fourth International Conference on Electromagnetic Wave Interaction with Water and Moist Substances, Weimar, Germany, 2001, (unpublished), pp. 165–172.
[25] S. R. J. Axelsson, IEEE Trans. Geosci. Remote Sens. **42**, 2370 (2004).
[26] J. Sachs, P. Peyerl, and M. Roßberg, *Proceedings of 16th IEEE Instrumentation and Measurement Technology Conference (IMTC)*, Venice, Italy, 24–26 May, 1999 (IEEE, New York, 1999), pp. 1390–1395.
[27] J. Sachs, *Ground Penetrating Radar*, IEE Radar, Sonar, Navigation, and Avionics Series 15, 2nd ed., edited by D. J. Daniels (Institution of Engineering and Technology, London, 2004), pp. 225–237.
[28] R. L. Peterson, R. E. Ziemer, and D. E. Borth, *Introduction to Spread Spectrum Communications* (Prentice-Hall, Englewood Cliffs, 1995).
[29] F. Thiel, F. Schubert, W. Hoffmann, and F. Seifert, *Proceedings of the 16th International Society of Magnetic Resonance in Medicine* (MIRA Digital, St. Louis, MO, 2008), p. 1054.
[30] F. Thiel, M. Hein, J. Sachs, U. Schwarz, and F. Seifert, *IEEE International Conference on Ultra-Wideband (ICUWB)*, Hanover, Germany, 2008 (IEEE, New York, 2008), Vol. 1, pp. 105–108.
[31] G. Ramachandran and M. Singh, Med. Biol. Eng. Comput. **27**, 525 (1989).
[32] S. Gabriel, R. W. Lau, and C. Gabriel, Phys. Med. Biol. **41**, 2251 and 2271 (1996).
[33] R. R. Shah, Drug Saf. **27**, 145 (2004).
[34] ICH Draft Consensus Guideline, (S7B). Safety Pharmacology Studies for Assessing the Potential for Delayed Ventricular Repolarization (QT Interval Prolongation) by Human Pharmaceuticals, 2002. http://www.ich.org/MediaServer.jser?@_ID_505&@_MODE_GLB.
[35] U. Steinhoff, S. Knappe-Grüneberg, A. Schnabel, F. Thiel, T. Schurig, M. Bader, and H. Koch, *Proceedings of the 14th International Conference on Biomagnetism*, 2004 (Biomag, Boston, 2004), pp. 375–376.